Bioconjugate Chemistry

Article

pubs.acs.org/bc

^{68}Ga-Labeled 3PRGD$_2$ for Dual PET and Cerenkov Luminescence Imaging of Orthotopic Human Glioblastoma

Di Fan,[†] Xin Zhang,[†] Lijun Zhong,[‡] Xujie Liu,[†] Yi Sun,[§] Huiyun Zhao,[†,‡] Bing Jia,[†] Zhaofei Liu,[†] Zhaohui Zhu,[§] Jiyun Shi,*[,†,∥] and Fan Wang*[,†,∥,⊥]

[†]Medical Isotopes Research Center and Department of Radiation Medicine, School of Basic Medical Sciences, [‡]Medical and Healthy Analytical Center, and [⊥]State Key Laboratory of Natural and Biomimetic Drugs, Center for Molecular and Translational Medicine, Peking University, Beijing 100191, China

[§]Department of Nuclear Medicine, Peking Union Medical College Hospital, Beijing 100857, China

[∥]Interdisciplinary Laboratory, Institute of Biophysics, Chinese Academy of Sciences, Beijing 100101, China

Supporting Information

ABSTRACT: β-Emitters can produce Cerenkov radiation that is detectable by Cerenkov luminescence imaging (CLI), allowing the combination of PET and CLI with one radiotracer for both tumor diagnosis and visual guidance during surgery. Recently, the clinical feasibility of CLI with the established therapeutic reagent Na^{131}I and the PET tracer ^{18}F-FDG was demonstrated. ^{68}Ga possesses a higher Cerenkov light output than ^{18}F and ^{131}I, which would result in higher sensitivity for CLI and improve the outcome of CLI in clinical applications. However, the research on ^{68}Ga-based tumor-specific tracers for CLI is limited. In this study, we examined the use of ^{68}Ga-radiolabeled DOTA-3PRGD$_2$ (^{68}Ga-3PRGD$_2$) for dual PET and CLI of orthotopic U87MG human glioblastoma. For this purpose, the Cerenkov efficiencies of ^{68}Ga and ^{18}F were measured with the IVIS Spectrum system (PerkinElmer, USA). The CLI signal intensity of ^{68}Ga was 15 times stronger than that of ^{18}F. PET and CLI of ^{68}Ga-3PRGD$_2$ were performed in U87MG human glioblastoma xenografts. Both PET and CLI revealed a remarkable accumulation of ^{68}Ga-3PRGD$_2$ in the U87MG human glioblastoma xenografts at 1 h p.i. with an extremely low background in the brain when compared with ^{18}F-FDG. Furthermore, ^{68}Ga-3PRGD$_2$ was used for dual PET and CLI of orthotopic human glioblastoma. The orthotopic human glioblastoma was clearly visualized by both imaging modalities. In addition, the biodistribution of ^{68}Ga-3PRGD$_2$ was assessed in normal mice to estimate the radiation dosimetry. The whole-body effective dose is 20.1 ± 3.3 μSv/MBq, which is equal to 3.7 mSv per whole-body PET scan with a 5 mCi injection dose. Thus, ^{68}Ga-3PRGD$_2$ involves less radiation exposure in patients when compared with ^{18}F-FDG (7.0 mSv). The use of ^{68}Ga-3PRGD$_2$ in dual PET and CLI shows great promise for tumor diagnosis and image-guided surgery.

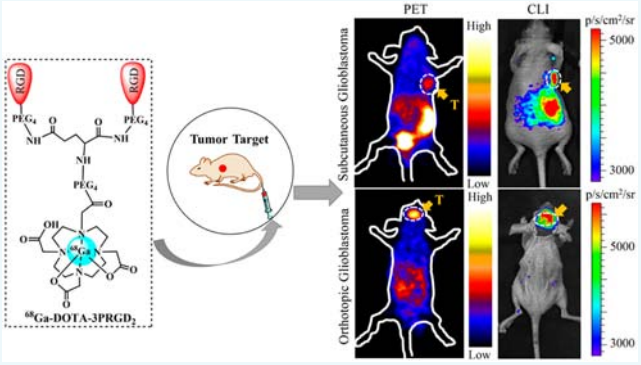

INTRODUCTION

Molecular imaging technologies have undergone explosive growth over the past few decades, and they now play a critical role in improving cancer diagnoses. Among these technologies, positron emission tomography (PET) enables high-sensitivity and quantitative imaging of the whole-body tracer distribution, which has proven to be valuable for tumor diagnostics and in surgical applications.[1,2] To strengthen the value of PET in clinical oncology, computed tomography (CT) and/or magnetic resonance imaging (MRI) have been combined with PET to provide detailed anatomical imaging.[3,4] Combining multiple imaging modalities harnesses the strengths of different imaging methods, which has become a very attractive strategy for in vivo studies and clinical applications.[5,6] PET/CT and PET/MRI are typically used to noninvasively assess diseased tissue prior to surgery; however, these techniques have not been broadly accepted within the operating suite. Optical imaging technologies used in conjunction with PET provide real-time tumor visualization and facilitate the process of intraoperative image-guided surgery (IGS).[7−9] Currently, however, the combination of PET and optical hybrid imaging is limited because of the lack of clinically approved targeted optical imaging agents.[10−12]

Cerenkov luminescence imaging (CLI) is an emerging optical imaging modality based on the detection of Cerenkov radiation induced by beta particles as they travel through biological tissues with a velocity faster than the speed of light.[13−15] CLI enables the use of widespread luminescence imaging equipment (IVIS Spectrum OI system) to visualize

Received: February 12, 2015
Published: April 8, 2015

DOI: 10.1021/acs.bioconjchem.5b00169
Bioconjugate Chem. 2015, 26, 1054−1060

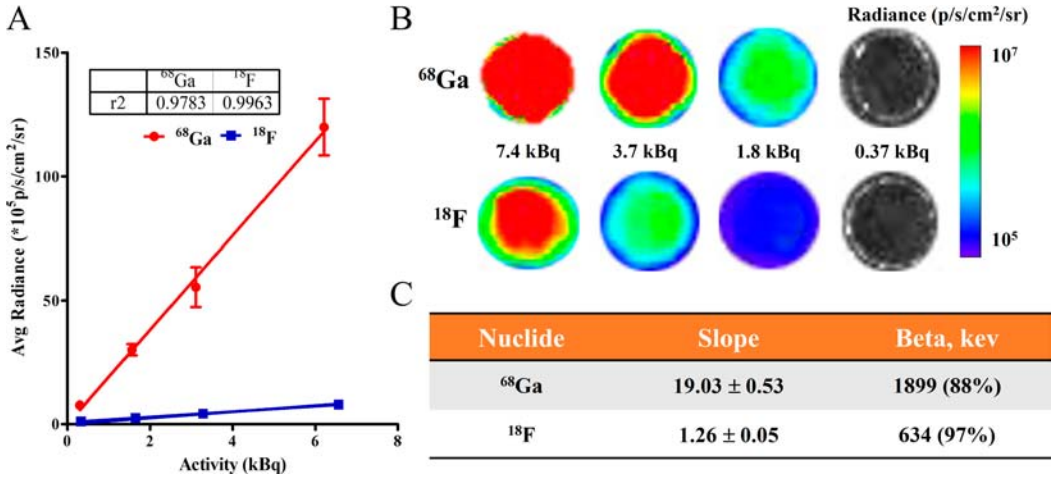

Figure 1. Correlation of the optical signals detected by the OI instruments and the radioactivity of the radionuclides ^{68}Ga and ^{18}F (A). The detection sensitivity of different radionuclides (^{68}Ga and ^{18}F) within a range as low as 0.37−7.40 kBq (0.01−0.2 μCi) (B). ^{68}Ga had a stronger positron emission energy and a higher K value (slope) when compared with ^{18}F; thus, ^{68}Ga exhibited a stronger Cerenkov luminescence signal intensity (C).

many commonly used medical isotopes, including clinical diagnostic (almost all PET radioisotopes) and therapeutic radionuclides.[16,17] Compared to conventional optical imaging agents, CLI has significant advantages, such as the use of approved radiotracers and the lack of an incident light source, which would result in its rapid translation to clinical applications combining PET imaging and CLI-guided surgery with PET tracers.[18]

Several studies have demonstrated that there is an excellent correlation between CLI and PET imaging signals;[17−19] furthermore, studies from Spinelli et al.[20] and Thorek et al.[21] have demonstrated the clinical feasibility of CLI with an established therapeutic reagent Na^{131}I and the PET tracer ^{18}F-FDG. Radionuclides emitting high-energy β^+/β^- particles exhibit high luminescence signals, and the number of Cerenkov radiation photons produced per disintegration follows the trend of ^{90}Y > ^{68}Ga > ^{15}O > ^{11}C > ^{124}I > ^{89}Zr > ^{18}F > ^{131}I > ^{64}Cu.[17−19] According to this specific tendency, the sensitivity of CLI can be improved enormously by using high Cerenkov light output isotopes, such as ^{90}Y and ^{68}Ga. ^{68}Ga is a positron-emitting radionuclide that has a markedly higher Cerenkov light output than ^{18}F; in addition, it is readily available from a long-shelf-life ^{68}Ge/^{68}Ga-generator with the parent ^{68}Ge ($t_{1/2}$ = 270 days) and easy to implement in the clinic, which makes it an excellent candidate for dual-modality PET and Cerenkov imaging.[22,23] Although ^{68}Ga-labeled targeting probes have been widely studied for PET imaging, ^{68}Ga-based tumor-specific tracers have not been extensively investigated for Cerenkov imaging application.[17,19,24]

Previously, we designed a novel RGD dimer PEG$_4$-E[PEG$_4$-c(RGDfK)]$_2$ (3PRGD$_2$) that specifically binds to integrin $\alpha_v\beta_3$/$\alpha_v\beta_5$ with relatively high affinity.[25−27] Radiolabeled 3PRGD$_2$ tracers have been successfully used for tumor detection in clinical pilot studies[28−30] and targeted radionuclide therapy in animal models.[31,32] Recently, we reported that ^{68}Ga-labeled DOTA-3PRGD$_2$ (^{68}Ga-3PRGD$_2$) could be used for neovascularization PET imaging to monitor the efficacy of anti-angiogenic therapies. Notably, ^{68}Ga-3PRGD$_2$ PET imaging reflected the tumor response to anti-angiogenic therapy much earlier and more accurately than ^{18}F-FDG PET imaging.[33] In addition, the analogue ^{68}Ga-PRGD$_2$ (PEG$_4$-E[c(RGDfK)]$_2$) was applied in a clinical pilot study for differentiating cases of high-grade glioma (HGG) from low-grade glioma (LGG).[34] This previous research highlights the potential of ^{68}Ga-3PRGD$_2$ for use in CLI applications. In the current study, we compared the use of ^{68}Ga-3PRGD$_2$ and ^{18}F-FDG for dual PET imaging and CLI of human glioblastoma xenografts; furthermore, we used dual PET imaging and CLI with ^{68}Ga-3PRGD$_2$ in orthotopic glioblastoma to demonstrate its potential use for tumor identification, tumor localization, and treatment guidance.

RESULTS

Chemistry and Radiochemistry of DOTA-3PRGD$_2$. DOTA-3PRGD$_2$ (Figure S1A) was prepared by direct conjugation of the 3PRGD$_2$ peptide with DOTA-OSu. The HPLC purity of DOTA-3PRGD$_2$ was >95%. The labeling was completed within 10−15 min with a decay-corrected yield ranging from 90% to 95%. After labeling, the specific activity of ^{68}Ga-labeled DOTA-3PRGD$_2$ (^{68}Ga-3PRGD$_2$) was typically approximately 5.5 MBq/nmol (0.15 Ci/μmol), with a radiochemical purity greater than 95% as determined by radio-HPLC (Figure S1B).

Measurement of Cerenkov Efficiency. To investigate whether ^{68}Ga is a suitable radionuclide for Cerenkov luminance imaging, we surveyed the detectability of varying amounts of ^{68}Ga using an IVIS Spectrum system. The ^{18}F radionuclide was used as a comparison for ^{68}Ga. Both tested radionuclides provided optical signals with good sensitivity over a 0.5−1 min acquisition time. Under the conditions utilized in our studies, good signal-to-noise (S/N) ratios were observed with 0.1 μCi of radioactivity for ^{18}F and ^{68}Ga. A plot of the average radiance vs the radioactive intensity for these two radionuclides provided the radionuclides' imaging sensitivity as a K value of the slope (Figure 1). ^{68}Ga showed a higher K value (slope = 19.03 ± 0.53) and stronger signal intensity than ^{18}F (slope = 1.26 ± 0.05). In addition, the in vitro images clearly showed that pure ^{68}Ga had a markedly higher sensitivity than ^{18}F. As expected, the optical photon intensity was greater with higher-energy β-emitters and was proportional to the radionuclide activity and increases with the refractive index of the medium.

PET and CLI with ^{18}F-FDG and ^{68}Ga-3PRGD$_2$ in a Glioblastoma Xenograft Model. ^{18}F-FDG and ^{68}Ga-3PRGD$_2$ were injected into mice bearing U87MG glioblasto-

DOI: 10.1021/acs.bioconjchem.5b00169
Bioconjugate Chem. 2015, 26, 1054−1060

mas. Next, the imaging was sequentially completed using microPET and the IVIS Spectrum system. Figure 2 presents a

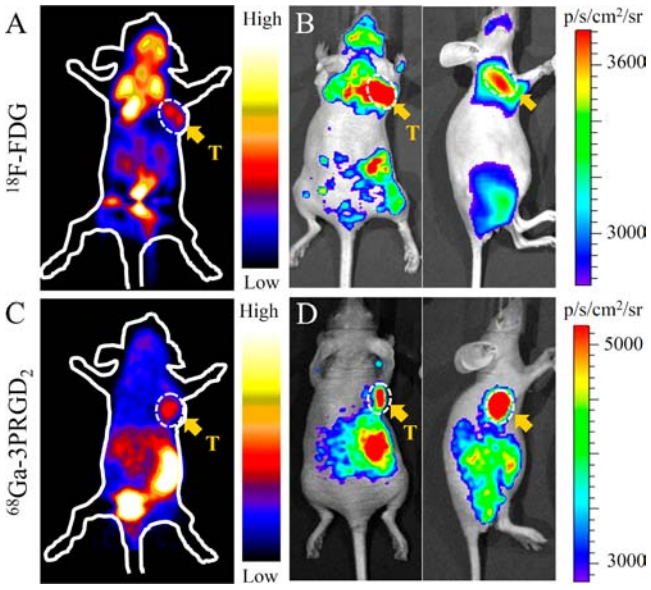

Figure 2. Representative PET (A) and CLI (B) images of ^{18}F-FDG in U87MG human glioblastoma-bearing mice at 60 min p.i. Representative PET (C) and CLI (D) images of ^{68}Ga-3PRGD$_2$ in U87MG human glioblastoma-bearing mice at 60 min p.i. Arrows indicate the location of the tumors.

qualitative comparison between the PET images and CLI images of the same mouse. ^{18}F-FDG was preferentially localized in U87MG tumors, as clearly shown in both the microPET imaging and the CLI images (Figure 2A,B). High signals from brown adipose tissue and brain tissue were observed using both modalities. Both PET imaging and CLI of ^{68}Ga-3PRGD$_2$ showed a significantly high tumor uptake with a high tumor-to-background ratio at 60 min p.i. (Figure 2C,D). As shown in Figure 2, both ^{68}Ga- and ^{18}F-based tracers can be used for CLI immediately after PET imaging. Even at 4 h p.i., the signal of 100 μCi of the ^{68}Ga or ^{18}F tracers was sufficient to perform the in vivo CLI (data not shown). Compared to images of ^{18}F-FDG, the images obtained using ^{68}Ga-3PRGD$_2$ showed markedly less background signal in the brown adipose tissue and the brain. The integrin receptor specificity of ^{68}Ga-3PRGD$_2$ was demonstrated using a blocking experiment. Almost no tracer was localized in the tumors after the blocking with excess cold RGD peptide (Figure S2).

Biodistribution of ^{18}F-FDG and ^{68}Ga-3PRGD$_2$ in a Glioblastoma Xenograft Model. ^{18}F-FDG and ^{68}Ga-3PRGD$_2$ were injected into mice bearing U87MG glioblastomas for biodistribution study. As shown in Figure 3, ^{18}F-FDG (5.45 ± 1.18%ID/g) and ^{68}Ga-3PRGD$_2$ (4.32 ± 0.71%ID/g) showed comparable tumor uptake in this tumor model at 60 min p.i. However, the heart uptake (49.22 ± 15.07%ID/g) and brain uptake (5.33 ± 0.33%ID/g) of ^{18}F-FDG were much higher than that of ^{68}Ga-3PRGD$_2$ (0.71 ± 0.21%ID/g; 0.20 ± 0.07%ID/g), because they are high-metabolic-rate organs (Figure 3).

PET and CLI of ^{68}Ga-3PRGD$_2$ in Orthotopic Glioblastoma Model. In the orthotopic tumor model, the PET imaging showed that ^{68}Ga-3PRGD$_2$ was significantly localized in the brain area (Figure 4A−C). The blocking study demonstrated that uptake in the brain area was very low.

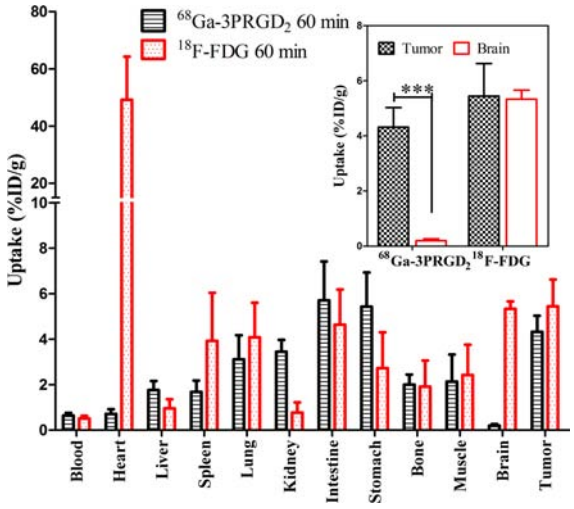

Figure 3. Biodistribution of ^{68}Ga-3PRGD$_2$ and ^{18}F-FDG in U87MG human glioblastoma-bearing mice at 60 min p.i. Data are expressed as %ID/g (n = 4, mean ± SD). ***: P < 0.0001.

With its high spatial resolution, PET can provide the coronal, sagittal, and transverse images of the orthotopic glioblastoma. CLI of the orthotopic model with ^{68}Ga-3PRGD$_2$ also showed a high tumor localization in the brain (Figure 4D). To further characterize the localization of ^{68}Ga-3PRGD$_2$ by CLI, the mice were euthanized and tumors were excised from the brain based on the CLI signal (Figure 4E). The brain tumors were further analyzed using H&E staining (Figure 4F).

Dose Safety and Pharmacokinetic Properties of ^{68}Ga-3PRGD$_2$. To investigate the dose safety and in vivo behavior of ^{68}Ga-3PRGD$_2$, we conducted a biodistribution study in normal female BALB/c mice. As shown in Figure S3, ^{68}Ga-3PRGD$_2$ dispersed quickly and broadly to all tested tissues within 10 min p.i. A rapid clearance from the circulation resulted in only a small amount of ^{68}Ga-3PRGD$_2$ remaining in the blood at 30 min p.i. The radiation dosimetry was calculated from the biodistribution data of ^{68}Ga-3PRGD$_2$ in normal mice using OLINDA-EXM software. The whole-body effective dose was 20.1 ± 3.3 μSv/MBq, which is equal to 3.7 mSv per whole-body PET scan with an injection dose of 5 mCi (Table 1).

DISCUSSION

Positron emission tomography (PET) and optical imaging (OI) are two of the most important imaging modalities.[2,3S] The combination of these techniques can be used to identify and localize tumors with PET while enabling intraoperative image-guided surgery (IGS) with the OI system.[9,12,18] Conventional PET/OI dual-modality molecular probes consist of a PET nuclide and a fluorescent chromophore.[11,12] Introducing a fluorophore into the probe is likely to increase the difficulty of chemical synthesis and water insolubility. Moreover, the clinically approved fluorescent chromophore-based optical imaging agents are rare, which hinders the translation of the conventional optical molecular probes to clinical use. Cerenkov luminescence imaging (CLI) has built a bridge between PET imaging and optical imaging and makes this dual-modality imaging achievable in the clinic. Recent advances in CLI have made it an excellent tool for both small-animal research and clinical applications. Spinelli et al. performed the first human Cerenkography in a patient after the injection of therapeutic Na^{131}I for hyperthyroidism and showed that it is possible to

DOI: 10.1021/acs.bioconjchem.5b00169
Bioconjugate Chem. 2015, 26, 1054−1060

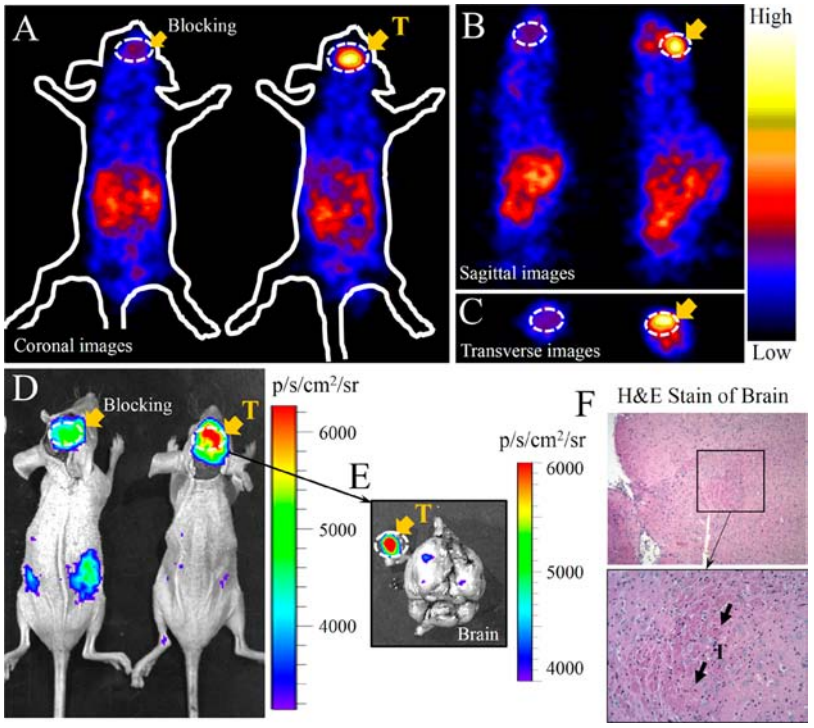

Figure 4. Representative PET (A–C) and CLI (D) images of ^{68}Ga-3PRGD$_2$ in an orthotopic U87MG human glioblastoma model at 60 min p.i. CLI images of an ex vivo brain and tumor (E). H&E staining of the brain (F). Arrows indicate the location of the tumors.

Table 1. Human Absorbed Dose Estimates of ^{68}Ga-3PRGD$_2$ Obtained from Normal White Mice[a]

target organ	effective dose (mean ± SD, N = 4) (mSv/MBq)
adrenals	$2.02 \times 10^{-05} \pm 3.07 \times 10^{-06}$
brain	$6.12 \times 10^{-06} \pm 8.88 \times 10^{-07}$
breasts	$9.61 \times 10^{-05} \pm 2.02 \times 10^{-05}$
LLI wall	$7.02 \times 10^{-04} \pm 1.65 \times 10^{-04}$
small intestine	$4.81 \times 10^{-04} \pm 1.22 \times 10^{-04}$
stomach wall	$7.08 \times 10^{-04} \pm 1.08 \times 10^{-04}$
ULI wall	$3.52 \times 10^{-05} \pm 7.77 \times 10^{-06}$
heart wall	$4.19 \times 10^{-03} \pm 1.11 \times 10^{-03}$
kidneys	$8.36 \times 10^{-04} \pm 1.26 \times 10^{-04}$
liver	$1.55 \times 10^{-03} \pm 2.25 \times 10^{-04}$
lungs	$6.96 \times 10^{-03} \pm 1.95 \times 10^{-03}$
muscle	$9.96 \times 10^{-06} \pm 2.01 \times 10^{-06}$
pancreas	$2.17 \times 10^{-05} \pm 3.44 \times 10^{-06}$
red marrow	$1.44 \times 10^{-03} \pm 1.38 \times 10^{-04}$
osteogenic cells	$1.07 \times 10^{-04} \pm 1.02 \times 10^{-05}$
skin	$1.29 \times 10^{-05} \pm 1.89 \times 10^{-06}$
spleen	$5.16 \times 10^{-03} \pm 1.34 \times 10^{-03}$
thymus	$6.98 \times 10^{-06} \pm 1.81 \times 10^{-06}$
thyroid	$4.45 \times 10^{-05} \pm 8.69 \times 10^{-06}$
urinary bladder wall	$1.20 \times 10^{-04} \pm 2.61 \times 10^{-05}$
total body	$2.01 \times 10^{-02} \pm 3.29 \times 10^{-03}$

[a]Note:The whole-body effective dose is 20.1 ± 3.3 μSv/MBq, which is equivalent to 3.7 mSv for a whole-body PET scan using a 5 mCi injection.

obtain a planar image of Cerenkov photons escaping from human tissue.[20] ^{18}F-FDG is the most widely used clinical PET tracer, and it has been used for clinical CLI. Thorek et al. demonstrated the feasibility of CLI in the detection of nodal disease in patients undergoing diagnostic ^{18}F-FDG scans.[21] Although the CLI technology has been shown to be feasible in a clinical setting, how to enhance the sensitivity of CLI is still a concern.

Higher-energy positron emitters produce more Cerenkov radiation photons, which have the potential to increase the sensitivity of CLI. Compared to ^{18}F, ^{68}Ga has markedly more β^+ energy (1.92 MeV vs 0.635 MeV), making it an excellent candidate for Cerenkov luminescence imaging.[19,22] In this study, the Cerenkov efficiency of ^{68}Ga and ^{18}F was measured. As shown in Figure 1, the radiance and activity of ^{68}Ga displays a linear relationship with an r^2 = 0.9783. The slope is approximately 15 times higher than that of ^{18}F; in other words, the light output of ^{68}Ga is 15 times higher than that of ^{18}F. The lowest tested activity of a ^{68}Ga-3PRGD$_2$ injection to acquire sufficient signal for CLI at 1 h p.i. was 40 μCi, which is much lower than that used for ^{18}F (100 μCi). Therefore, ^{68}Ga provides higher sensitivity and a shorter acquisition time. Unlike ^{18}F, ^{68}Ga can be readily labeled to tumor-targeting biomolecules via chelators (such as DOTA) to act as a tumor-specific probe. As shown in Figure 2A, ^{18}F-FDG PET imaging is hindered by a high background in high-activity tissues, such as the heart, brown fat pads, and the brain, due to its glucose metabolism-based accumulation mechanisms. ^{68}Ga-labeled 3PRGD$_2$ is a tumor-specific probe that may be a better choice for tumor identification in these tissues. As shown in Figure 2C, ^{68}Ga-3PRGD$_2$ PET imaging clearly visualizes glioblastoma xenograft tumors, and has a much clearer background in the brain when compared with PET imaging using ^{18}F-FDG. The CLI was acquired from the same mice immediately after PET imaging; thus, the CLI results for ^{18}F-FDG and ^{68}Ga-3PRGD$_2$ in the glioblastoma xenografts were consistent with the PET findings (Figure 2B,D). The biodistribution data in the glioblastoma xenograft tumor model confirmed the imaging findings. As shown in Figure 3, the tumor-to-brain ratio of ^{68}Ga-3PRGD$_2$ uptake (24.51 ± 10.97) is about 20 times that of

DOI: 10.1021/acs.bioconjchem.5b00169
Bioconjugate Chem. 2015, 26, 1054–1060

^{18}F-FDG (1.03 ± 0.28). These data suggest that ^{68}Ga-3PRGD$_2$ may be more promising for orthotopic glioblastoma detection than ^{18}F-FDG.

To study the potential of ^{68}Ga-3PRGD$_2$ for the detection of orthotopic glioblastoma, an orthotopic U87MG human glioblastoma mouse model was established. With the clear background of ^{68}Ga-3PRGD$_2$ in the brain, the orthotopic brain tumor was distinctly localized by ^{68}Ga-3PRGD$_2$ PET imaging in coronal, sagittal, and transverse images. The tumor was also clearly visualized in the brain by CLI. A blocking experiment was performed to confirm the specific targeting of ^{68}Ga-3PRGD$_2$ to the orthotopic brain tumors. As shown in Figure 4E, the tumor was excised based on the CLI signal, which suggests that the ^{68}Ga-3PRGD$_2$ holds great potential for application in the image-guided surgery of orthotopic glioblastomas. Surgery to remove the tumor is typically the first option once a brain tumor has been diagnosed. Based on conventional diagnostic imaging, it is challenging, even for the very experienced surgeons to precisely remove a brain tumor without damage to healthy brain tissue. Unlike separated PET and optical images using different probes, PET and CLI dual-modality imaging with a single probe, such as ^{68}Ga-3PRGD$_2$, allows the surgeon to detect the tumor location with PET and then provide visual guidance of the tumor boundaries via CLI using the same injected dose during surgery. This combination of techniques ensures that the imaging signal from both modalities refers to the same spot and guarantees that the surgeon can remove the tumor without damaging healthy tissue. Holland et al. have reported the first demonstration of the feasibility of using CLI of ^{89}Zr-DFO-trastuzumab for image-guided intraoperative surgical resection of tumors.[36] Chen et al. have also demonstrated the feasibility of using fiber-based Cerenkov luminescence endoscopy of ^{18}F-FDG for image-guided surgery.[37] Here, we emphasize the advantages of using ^{68}Ga for Cerenkov imaging, and provide a new candidate of ^{68}Ga-3PRGD$_2$ for the specific tumor detection and CLI-guided surgery of glioblastoma. In addition, the estimated absorbed radiation dose of ^{68}Ga-3PRGD$_2$ was 3.7 mSv for a whole-body PET scan with a 5 mCi injection dose (Table 1). This value is much lower than the effective dose of the currently used clinical PET tracer ^{18}F-FDG (~7.0 mSv for a whole-body PET scan with a 10 mCi injection dose) and demonstrates the safety of ^{68}Ga-3PRGD$_2$ for clinical use.[38,39]

■ CONCLUSION

^{68}Ga has many advantages over ^{18}F in Cerenkov luminescence imaging (CLI), and it may afford a variety of novel optical imaging applications with PET radiopharmaceuticals. Both PET and CLI of ^{68}Ga-3PRGD$_2$ revealed a remarkable accumulation of ^{68}Ga-3PRGD$_2$ in orthotopic glioblastoma at 1 h p.i. with an extremely low background. In addition, ^{68}Ga-3PRGD$_2$ resulted in lower radiation exposure for patients compared with ^{18}F-FDG. Dual PET and CLI using ^{68}Ga-3PRGD$_2$ is not only very promising for tumor diagnosis but also has great potential for use in image-guided surgeries for orthotopic glioblastomas or other superficial tumors. Thus, dual PET and CLI with ^{68}Ga-3PRGD$_2$ may be rapidly translated into clinical practice in the future.

■ EXPERIMENTAL SECTION

Chemicals. All commercially available chemical reagents purchased from J. T. Baker (USA) were of analytical grade. The bifunctional chelator 1,4,7,10-tetraazacyclododecane-1,4,7,10-tetraacetic acid mono (*N*-hydroxysuccinimide ester) (DOTA-NHS-Ester) was purchased from Macrocyclics, Inc. (Dallas, TX). Chelex 100 resin (50−100 mesh) was purchased from Sigma-Aldrich (St. Louis, MO). Water and all buffers were passed through a Chelex 100 column (1 × 15 cm) before use for DOTA conjugation and radiolabeling to ensure that all aqueous buffers were metal free. The peptide PEG$_4$-E[PEG$_4$-c(RGDfK)]$_2$ (3PRGD$_2$) was synthesized by Peptides International (Louisville, KY). The ^{68}GaCl$_3$ solution was obtained from a commercially available ^{68}Ge/^{68}Ga generator (ITG Isotope Technologies Garching GmbH, Garching, Germany). The reversed-phase high-performance liquid chromatography (HPLC) system was the same as that previously described.[40] HPLC method 1 (for conjugation): The flow rate was 4.0 mL/min. The mobile phase was isocratic with 100% solvent A (DD Water +0.05% TFA) and 0% solvent B (Acetonitrile +0.05% TFA) at 0 min, followed by a gradient mobile phase going to 60% solvent B at 30 min. HPLC method 2 (for radiolabeling): The flow rate was 1.0 mL/min. The mobile phase was isocratic with 95% solvent A (DD Water +0.05% TFA) and 5% solvent B (Acetonitrile +0.05% TFA) at 0 min, followed by a gradient mobile phase going to 15% solvent B at 15 min, then back to 5% solvent B at 20 min. ^{18}F-FDG was obtained from the Department of Nuclear Medicine, Peking Union Medical College Hospital.

Cell Culture and Animal Models. The human glioblastoma cell line U87MG (ATCC HTB-14) was purchased from American Type Culture Collection (Manassas, VA). U87MG cells were cultured in low-glucose Dulbecco's modified Eagle's medium (DMEM) supplemented with 10% (v/v) fetal bovine serum (FBS) at 37 °C in a humidified atmosphere with 5% CO_2. Female BALB/c nude mice (4−6 weeks of age) were purchased from the Department of Experimental Animals, Peking University Health Science Center. All animal experiments were performed in accordance with the guidelines of Institutional Animal Care and Use Committee (IACUC) of Peking University. The xenografted tumor model was established by subcutaneous injection of 2 × 10^6 tumor cells into the right flank. When the tumor volume reached 200−300 mm^3 (3−4 weeks after inoculation), the tumor-bearing nude mice were used for imaging studies. The orthotopic tumor model was established by intracranial injection of ~10^5 U87MG tumor cells into the frontal white matter of nude mice.

Synthesis of DOTA-3PRGD$_2$. DOTA-3PRGD$_2$ conjugate was prepared as previously described.[33] Briefly, DOTA-NHS (6 μmol, calculated on the basis of *N*-hydroxysulfonosuccinimide) was added to the peptides (2 μmol) in 0.2 N $NaHCO_3$ solution (pH 8.5). After stirring at 37 °C overnight, the DOTA conjugate was isolated by semipreparative HPLC. HPLC analysis and mass spectroscopy were used to confirm the identity of the product.

Preparation of ^{68}Ga-3PRGD$_2$. A ^{68}GaCl$_3$ solution was eluted from the ^{68}Ge/^{68}Ga generator in 4 × 1 mL 0.05 M HCl vials, and the ^{68}GaCl$_3$ obtained in the second 1 mL vial was directly used for radiolabeling without further purification. For ^{68}Ga radiolabeling, 1.0 mL of a ^{68}GaCl$_3$ solution (370 MBq) was added to a lyophilized kit containing sodium acetate (50 μmol) and DOTA-3PRGD$_2$ (10 nmol). Next, the solution was incubated in a metal bath at 100 °C for 10−15 min. After cooling to room temperature over 5 min, the ^{68}Ga-labeled DOTA-3PRGD$_2$ (^{68}Ga-3PRGD$_2$) was subjected to radio-HPLC analysis. The product was then formulated in phosphate-

DOI: 10.1021/acs.bioconjchem.5b00169
Bioconjugate Chem. 2015, 26, 1054−1060

buffered saline (PBS) and passed through a 0.22 μm Millipore filter into a sterile multidose vial for use in the in vivo experiments.

Measurement of the Cerenkov Efficiency. The Cerenkov efficiency was measured with an IVIS Spectrum system (PerkinElmer, USA). For this study, ^{18}F-FDG and $^{68}GaCl_3$ were diluted with PBS to different concentrations (0.01, 0.05, 0.1, and 0.2 μCi) and then added into a flat-bottom 96-well plate (Nunc, Naperville, IL) in triplicate for each concentration. The total volume in each well was standardized to 250 μL. Images were acquired and analyzed using *Living Image 4.2* software (PerkinElmer, USA). The quantification of Cerenkov radiation images was corrected in accordance with the respective physical decay properties of the radionuclides. The optical signal was normalized to photons per second per square centimeter per steradian (p/s/cm^2/sr). An identical setting was used for the in vivo CLI.

Biodistribution in U87MG Xenograft Tumor Model. Eight U87MG tumor-bearing mice were randomly divided into two groups of four animals each. A dose of 50 μCi ^{68}Ga-3PRGD$_2$ (in 0.1 mL saline) or 50 μCi ^{18}F-FDG (in 0.1 mL saline) was administered intravenously to each mouse. The biodistribution studies were carried out by euthanizing the mice at 60 min p.i. The blood, heart, liver, spleen, lung, kidney, stomach, intestine, muscle, bone, brain, and tumor were harvested, weighed, and measured for radioactivity in a γ-counter. The organ uptake was calculated as a percentage of the injected dose per gram of wet tissue mass (%ID/g).

MicroPET Imaging. Small-animal microPET imaging was performed using a small-animal PET R4 rodent model scanner (Siemens Medical Solutions USA, Inc., Knoxville, TN) and a tail-vein injection of approximately 3.70 MBq (~100 μCi) of ^{18}F-FDG or 1.48−3.70 MBq (40−100 μCi)^{68}Ga-3PRGD$_2$ into BALB/c nude mice bearing U87MG xenografts under isoflurane anesthesia (Abbott Laboratories, Shanghai) (n = 4/group). The PET imaging of the orthotopic U87MG xenografts was only performed with ^{68}Ga-3PRGD$_2$. At 1 h postinjection (p.i.), the mice were placed in the prone position near the center of the field of view (FOV) of the small-animal PET scanner. Ten-minute static PET images were acquired, and the images were reconstructed according to a two-dimensional ordered-subsets expectation maximum (OSEM) algorithm. No correction was necessary for attenuation or scattering. The integrin receptor specificity of ^{68}Ga-3PRGD$_2$ was demonstrated using a blocking experiment. Briefly, we coinjected excess cold RGD peptide (~500 μg) along with the tracer in mice assigned to the blocking group.

Cerenkov Luminescence Imaging. For the in vivo imaging studies, mice bearing U87MG xenografts were injected via the tail vein with ^{18}F-FDG (~100 μCi) or ^{68}Ga-3PRGD$_2$ (~100 μCi) 1 h before the PET/CLI acquisition. The CLI studies of the orthotopic U87MG xenografts were only performed with ^{68}Ga-3PRGD$_2$. The CLI studies were performed immediately after the corresponding PET with an IVIS Spectrum system. Acquisition and analysis of the images were carried out using *Living Image 3.0* software (Caliper Life Sciences). Wavelength-resolved spectral imaging was performed using an 18-set narrow-band emission filter (490−850 nm). Animals were placed in a light-tight chamber under isofluorane anesthesia. Each acquisition, with or without filters, took 1−5 min for all studies. The images were acquired and analyzed using *Living Image 3.0* software (Caliper life sciences, Hopkinton, MA). The optical signal was normalized to photons per second per square centimeter per steradian (p/s/cm^2/sr). Cerenkov imaging of orthotopic glioblastoma was done after cutting the head skin, to get a good look at the brain and tumor by eyes. The cranial bone was not removed until we took out the brain for partial imaging.

Dose Safety and Pharmacokinetic Properties of ^{68}Ga-3PRGD$_2$. A total of 20 BALB/c normal mice were randomly divided into five groups of four animals each. A dose of 50 μCi ^{68}Ga-3PRGD$_2$ (in 0.1 mL saline) was administered intravenously to each mouse. Time-dependent biodistribution studies were carried out by euthanizing the mice at 10, 30, 60, 120, and 240 min p.i. The blood, heart, liver, spleen, lung, kidney, stomach, intestine, muscle, bone, and brain were harvested, weighed, and measured for radioactivity in a γ-counter. The organ uptake was calculated as a percentage of the injected dose per gram of wet tissue mass (%ID/g). The human absorbed doses in normal organs for ^{68}Ga-3PRGD$_2$ were estimated from the biodistribution data in normal mice using dedicated software (OLINDA/EXM).

■ ASSOCIATED CONTENT

Supporting Information

Chemical structure (Figure S1), PET and CLI images (Figure S2), and biodistribution bar charts (Figure S3). This material is available free of charge via the Internet at http://pubs.acs.org.

■ AUTHOR INFORMATION

Corresponding Authors

*E-mail: shijiyun@moon.ibp.ac.cn. Tel.: 86-10-82802537. Fax: 86-10-82802871.

*E-mail: wangfan@bjmu.edu.cn. Tel.: 86-10-82802871. Fax: 86-10-82801145.

Notes

The authors declare no competing financial interest.

■ ACKNOWLEDGMENTS

This research was supported by the National Natural Science Foundation of China (NSFC) projects (81125011, 81321003, 81420108019, 81427802, and 81201127), grant from Beijing Natural Science Foundation (7142086). J. Shi would like to thank Luzheng Xu for excellent technical support.

■ REFERENCES

(1) Phelps, M. E. (2000) PET: the merging of biology and imaging into molecular imaging. *J. Nucl. Med. 41*, 661−81.

(2) Phelps, M. E. (2000) Positron emission tomography provides molecular imaging of biological processes. *Proc. Natl. Acad. Sci. U. S. A. 97*, 9226−9233.

(3) Histed, S. N., Lindenberg, M. L., Mena, E., Turkbey, B., Choyke, P. L., and Kurdziel, K. A. (2012) Review of functional/anatomical imaging in oncology. *Nucl. Med. Commun. 33*, 349−61.

(4) Judenhofer, M. S., Wehrl, H. F., Newport, D. F., Catana, C., Siegel, S. B., Becker, M., Thielscher, A., Kneilling, M., Lichy, M. P., Eichner, M., et al. (2008) Simultaneous PET-MRI: a new approach for functional and morphological imaging. *Nat. Med. 14*, 459−465.

(5) Antoch, G., Vogt, F. M., Freudenberg, L. S., Nazaradeh, F., Goehde, S. C., Barkhausen, J., Dahmen, G., Bockisch, A., Debatin, J. F., and SG, R. (2003) WHole-body dual-modality pet/ct and whole-body mri for tumor staging in oncology. *J. Am. Med. Assoc. 290*, 3199−3206.

(6) Pichler, B. J., Kolb, A., Nagele, T., and Schlemmer, H. P. (2010) PET/MRI: paving the way for the next generation of clinical multimodality imaging applications. *J. Nucl. Med. 51*, 333−6.

(7) Keereweer, S., Kerrebijn, J. D., van Driel, P. B., Xie, B., Kaijzel, E. L., Snoeks, T. J., Que, I., Hutteman, M., van der Vorst, J. R., Mieog, J.

DOI: 10.1021/acs.bioconjchem.5b00169
Bioconjugate Chem. 2015, 26, 1054−1060

S., et al. (2011) Optical image-guided surgery–where do we stand? *Mol. Imaging Biol. 13*, 199−207.
(8) Pruliere-Escabasse, V., and Coste, A. (2010) Image-guided sinus surgery. *European Annals of Otorhinolaryngology, Head and Neck Diseases 127*, 33−9.
(9) Gibbs, S. L. (2012) Near infrared fluorescence for image-guided surgery. *Quantitative Imaging in Medicine and Surgery 2*, 177−87.
(10) Keereweer, S., Van Driel, P. B., Snoeks, T. J., Kerrebijn, J. D., Baatenburg de Jong, R. J., Vahrmeijer, A. L., Sterenborg, H. J., and Lowik, C. W. (2013) Optical image-guided cancer surgery: challenges and limitations. *Clin. Cancer Res. 19*, 3745−54.
(11) Nahrendorf, M., Keliher, E., Marinelli, B., Waterman, P., Feruglio, P. F., Fexon, L., Pivovarov, M., Swirski, F. K., Pittet, M. J., Vinegoni, C., et al. (2010) Hybrid PET-optical imaging using targeted probes. *Proc. Natl. Acad. Sci. U.S.A. 107*, 7910−5.
(12) Seibold, U., Wangler, B., Schirrmacher, R., and Wangler, C. (2014) Bimodal imaging probes for combined PET and OI: recent developments and future directions for hybrid agent development. *BioMed. Res. Int. 2014*, 153741.
(13) Thorek, D., Robertson, R., Bacchus, W. A., Hahn, J., Rothberg, J., Beattie, B. J., and Grimm, J. (2012) Cerenkov imaging - a new modality for molecular imaging. *Am. J. Nucl. Med. Mol. Imaging 2*, 163−73.
(14) Dothager, R. S., Goiffon, R. J., Jackson, E., Harpstrite, S., and Piwnica-Worms, D. (2010) Cerenkov radiation energy transfer (CRET) imaging: a novel method for optical imaging of PET isotopes in biological systems. *PLoS One 5*, e13300.
(15) Mitchell, G. S., Gill, R. K., Boucher, D. L., Li, C., and Cherry, S. R. (2011) In vivo Cerenkov luminescence imaging: a new tool for molecular imaging. *Philos. Trans. R. Soc., A 369*, 4605−19.
(16) Ruggiero, A., Holland, J. P., Lewis, J. S., and Grimm, J. (2010) Cerenkov luminescence imaging of medical isotopes. *J. Nucl. Med. 51*, 1123−30.
(17) Liu, H., Ren, G., Miao, Z., Zhang, X., Tang, X., Han, P., Gambhir, S. S., and Cheng, Z. (2010) Molecular optical imaging with radioactive probes. *PloS one 5*, e9470.
(18) Xu, Y., Liu, H., and Cheng, Z. (2011) Harnessing the power of radionuclides for optical imaging: Cerenkov luminescence imaging. *J. Nucl. Med. 52*, 2009−18.
(19) Steinberg, J. D., Raju, A., Chandrasekharan, P., Yang, C. T., Khoo, K., Abastado, J. P., Robins, E. G., and Townsend, D. W. (2014) Negative contrast Cerenkov luminescence imaging of blood vessels in a tumor mouse model using [68Ga]gallium chloride. *EJNMMI Research 4*, 15.
(20) Spinelli, A. E., Ferdeghini, M., Cavedon, C., Zivelonghi, E., Calandrino, R., Fenzi, A., Sbarbati, A., and Boschi, F. (2013) First human Cerenkography. *J. Biomed. Opt. 18*, 20502.
(21) Thorek, D. L., Riedl, C. C., and Grimm, J. (2014) Clinical Cerenkov luminescence imaging of ^{18}F-FDG. *J. Nucl. Med. 55*, 95−8.
(22) Fani, M., Andre, J. P., and Maecke, H. R. (2008) ^{68}Ga-PET: a powerful generator-based alternative to cyclotron-based PET radiopharmaceuticals. *Contr. Media Mol. Imaging 3*, 67−77.
(23) Boschi, S., Malizia, C., and Lodi, F. (2013) Overview and perspectives on automation strategies in (68)Ga radiopharmaceutical preparations. *Recent Results Cancer Res. 194*, 17−31.
(24) Nedrow, J. R., White, A. G., Modi, J., Nguyen, K., Chang, A. J., and Anderson, C. J. (2014) Positron emission tomographic imaging of copper 64- and gallium 68-labeled chelator conjugates of the somatostatin agonist tyr3-octreotate. *Mol. Imaging 13*.
(25) Wang, L., Shi, J., Kim, Y. S., Zhai, S., Jia, B., Zhao, H., Liu, Z., Wang, F., Chen, X., and Liu, S. (2009) Improving tumor-targeting capability and pharmacokinetics of (99m)Tc-labeled cyclic RGD dimers with PEG(4) linkers. *Mol. Pharmaceutics 6*, 231−45.
(26) Shi, J., Kim, Y. S., Zhai, S., Liu, Z., Chen, X., and Liu, S. (2009) Improving tumor uptake and pharmacokinetics of (64)Cu-labeled cyclic RGD peptide dimers with Gly(3) and PEG(4) linkers. *Bioconjugate Chem. 20*, 750−9.
(27) Shi, J., Kim, Y. S., Chakraborty, S., Jia, B., Wang, F., and Liu, S. (2009) 2-Mercaptoacetylglycylglycyl (MAG2) as a bifunctional chelator for 99mTc-labeling of cyclic RGD dimers: effect of technetium chelate on tumor uptake and pharmacokinetics. *Bioconjugate Chem. 20*, 1559−68.
(28) Zhu, Z., Miao, W., Li, Q., Dai, H., Ma, Q., Wang, F., Yang, A., Jia, B., Jing, X., Liu, S., et al. (2012) 99mTc-3PRGD2 for integrin receptor imaging of lung cancer: a multicenter study. *J. Nucl. Med. 53*, 716−22.
(29) Zhao, D., Jin, X., Li, F., Liang, J., and Lin, Y. (2012) Integrin alphavbeta3 imaging of radioactive iodine-refractory thyroid cancer using 99mTc-3PRGD2. *J. Nucl. Med. 53*.
(30) Ma, Q., Ji, B., Jia, B., Gao, S., Ji, T., Wang, X., Han, Z., and Zhao, G. (2011) Differential diagnosis of solitary pulmonary nodules using (99m)Tc-3P(4)-RGD(2) scintigraphy. *Eur. J. Nucl. Med. Mol. Imaging 38*, 2145−52.
(31) Shi, J., Fan, D., Dong, C., Liu, H., Jia, B., Zhao, H., Jin, X., Liu, Z., Li, F., and Wang, F. (2014) Anti-tumor effect of integrin targeted (177)Lu-3PRGD2 and combined therapy with Endostar. *Theranostics 4*, 256−66.
(32) Liu, Z., Shi, J., Jia, B., Yu, Z., Liu, Y., Zhao, H., Li, F., Tian, J., Chen, X., Liu, S., et al. (2011) Two (90)Y-labeled multimeric RGD peptides RGD4 and 3PRGD2 for integrin targeted radionuclide therapy. *Mol. Pharmaceutics 8*, 591−9.
(33) Shi, J., Jin, Z., Liu, X., Fan, D., Sun, Y., Zhao, H., Zhu, Z., Liu, Z., Jia, B., and Wang, F. (2014) PET imaging of neovascularization with (68)Ga-3PRGD2 for assessing tumor early response to Endostar antiangiogenic therapy. *Mol. Pharmaceutics 11*, 3915−22.
(34) Li, D., Zhao, X., Zhang, L., Li, F., Ji, N., Gao, Z., Wang, J., Kang, P., Liu, Z., Shi, J., et al. (2014) (68)Ga-PRGD2 PET/CT in the evaluation of glioma: a prospective study. *Mol. Pharmaceutics 11*, 3923−9.
(35) Balas, C. (2009) Review of biomedical optical imaging—a powerful, non-invasive, non-ionizing technology for improving in vivo diagnosis. *Meas. Sci. Technol. 20*, 104020.
(36) Holland, J. P., Normand, G., Ruggiero, A., Lewis, J. S., and Grimm, J. (2011) Intraoperative imaging of positron emission tomographic radiotracers using Cerenkov luminescence emissions. *Mol. Imaging 10*, 1−3 177−86.
(37) Liu, H., Carpenter, C. M., Jiang, H., Pratx, G., Sun, C., Buchin, M. P., Gambhir, S. S., Xing, L., and Cheng, Z. (2012) Intraoperative imaging of tumors using Cerenkov luminescence endoscopy: a feasibility experimental study. *J. Nucl. Med. 53*, 1579−84.
(38) Jones, S. C., Alavi, A., Christman, D., Montanez, I., Wolf, A. P., and Reivich, M. (1982) The radiation dosimetry of 2 [F-18]fluoro-2-deoxy-D-glucose in man. *J. Nucl. Med. 23*, 613−7.
(39) Brix, G., Lechel, U., Glatting, G., Ziegler, S. I., Munzing, W., Muller, S. P., and Beyer, T. (2005) Radiation exposure of patients undergoing whole-body dual-modality 18F-FDG PET/CT examinations. *J. Nucl. Med. 46*, 608−13.
(40) Shi, J., Wang, L., Kim, Y. S., Zhai, S., Jia, B., Wang, F., and Liu, S. (2009) 99mTcO(MAG2−3G3-dimer): a new integrin alpha(v)-beta(3)-targeted SPECT radiotracer with high tumor uptake and favorable pharmacokinetics. *Eur. J. Nucl. Med. Mol. Imaging 36*, 1874−84.

DOI: 10.1021/acs.bioconjchem.5b00169
Bioconjugate Chem. 2015, 26, 1054−1060